Ultimate Light Trapping in a Free-Form Plasmonic Waveguide

Juho Park,[1] Sanmun Kim,[2] Joongwon Lee,[3] Sergey G. Menabde,[1,†] and Min Seok Jang[1,*]

[1] *School of Electrical Engineering, Korea Advanced Institute of Science and Technology, Daejeon 34141, Korea*
[2] *St. John's College, University of Cambridge, Cambridge CB2 1TP, United Kingdom*
[3] *School of Electrical and Computer Engineering, Cornell University, Ithaca, New York 14853, USA*

(Received 1 May 2019; revised manuscript received 5 July 2019; published 15 August 2019)

Slow light enables spatiotemporal manipulation of electromagnetic waves at the nanoscale and allows access to a plethora of nonlinear optical phenomena. Although the guided waves in plasmonic waveguides are known to inherently possess a slow energy velocity, their ultimate light-trapping performance remains unknown as the effect of the waveguide's shape alteration has not been considered systematically so far. In this work, we theoretically demonstrate a free-form optimized metal-insulator-metal plasmonic waveguide for light trapping that exhibits a quality factor several times higher than that of the conventional linearly tapered structures. The quality factor of the optimized waveguide saturates to the theoretical limit at a surprisingly short device length, which shows a nontrivial inverse logarithmic dependence on the material loss. The demonstrated design has a quality-factor-to-footprint ratio comparable to that of state-of-the-art photonic cavities.

DOI: 10.1103/PhysRevApplied.12.024030

I. INTRODUCTION

Slow or *trapped* light allows the time-domain processing of optical signals [1], spatial compression of electromagnetic fields [2], and access to nonlinear optical effects [3]. These phenomena are fundamental for the operation of many optical devices, such as optical switches, optical memory, and photonic integrated circuits [4]. Guided waves in plasmonic waveguides are inherently slow as their power flow in the metallic layer is in the opposite direction to the wave propagation. It has been shown that the energy flows in different layers of waveguides can completely cancel each other out, resulting in a vanishing energy velocity by careful choice of the refractive indices and thicknesses of the materials composing the waveguide [5]. This idea, a "trapped rainbow," has been investigated as a promising approach to slow down light in solid-state systems, including tapered waveguides [5–7], photonic crystals [8,9], and plasmonic gratings [10–12]. The light-trapping performance of linearly tapered waveguides has been studied quantitatively by analyzing the coupling behavior between the guided modes in the structure. As a result, it has been verified that a linear taper cannot trap light to a complete standstill even if the system is conservative, and its quality factor further drops as the material loss increases [13]. Researchers have suggested various approaches to increase the light-trapping efficiency in taper waveguides, such as improving the fabrication quality [6,8], carefully selecting the operating wavelength [10,14], reducing the intrinsic material-mediated loss of the waveguide [6,15], and compensating the Ohmic loss of the waveguide by introducing optical gain materials [16,17]. To date, however, most research efforts on trapped rainbows have assumed a simple linear waveguide geometry and never explored how altering the shape of the waveguide would affect the light-trapping performance.

In this work, we search for the optimal geometry of a free-form metal-insulator-metal (*M-I-M*) plasmonic waveguide for light trapping, and reveal its unique properties that are significantly different from those of the conventional linearly tapered structures. We optimize the waveguide geometry by using three different numerical optimization algorithms combined with the transfer-matrix method, and confirm the results with full-wave simulations based on the finite-element method (FEM). The optimized light-trapping structure possesses a dramatically enhanced quality factor, almost reaching the theoretical limit imposed by the material loss. It also exhibits a distinctive mode dynamics and a unique dependence on the material loss, both being fundamentally different from those of the conventional linearly tapered structures. Unlike linearly tapered waveguides, whose characteristic length (minimum necessary length to reach half of the maximum quality factor) is inversely proportional to the material loss, the quality factor of the optimized structure saturates at much shorter length, and its characteristic length scales logarithmically with the inverse material

*jang.minseok@kaist.ac.kr
†menabde@kaist.ac.kr

loss. Further, to demonstrate the feasibility of the proposed design approach, we analyze the optimization results obtained with realistic materials at visible and mid-IR frequencies.

II. RESULTS AND DISCUSSION

A. Mode dynamics in a *M-I-M* waveguide

Here we focus our discussion on the *M-I-M* three-layer waveguide configuration as it is one of the simplest rainbow trapping devices and is superior in terms of trapping efficiency to other three-layer configurations such as insulator-metal-insulator (*I-M-I*; see Sec. S5 of Supplemental Material [18] for the results and discussion of the *I-M-I* case) and insulator–negative-index-material–insulator structures [13]. A schematic of a *M-I-M* plasmonic waveguide with an arbitrary core profile is shown in Fig. 1(a). Throughout this paper, assuming operation at a single frequency, we set the permittivity of the dielectric core as $\epsilon_d = 10$ and that of the metal claddings as $\epsilon_m = -2 + \gamma i$, where γ corresponds to the Ohmic loss. The small negative permittivity of the metal can generally be achieved at frequencies slightly below the plasma frequency or near the phonon resonances of polar crystals. The geometry is assumed to have mirror symmetry with respect to the *y-z* plane and does not vary along the y direction. We perform the optimization by changing the waveguide's core thickness 2α along the z direction for the segment of finite length L [Fig. 1(a)]. The core thickness of the input ($2\alpha_{\text{in}}$) and output ($2\alpha_{\text{out}}$) ports of the waveguide segment, normalized to the free-space wave number k_0, are fixed at $\alpha_{\text{in}}k_0 = 0.648$ and $\alpha_{\text{out}}k_0 = 0.616$, respectively. These values are selected to encompass the thicknesses associated with the degeneracy point (α_d) and mode cutoff (α_c) for the two TM_2 modes of the waveguide [Figs. 1(b) and 1(c)] [13], the importance of which will become evident in Sec. 2.4.

Under the condition $\sqrt{|\varepsilon_d/\varepsilon_m|} + \arctan\left(\sqrt{|\varepsilon_d/\varepsilon_m|}\right) > \pi$, the *M-I-M* waveguide supports two TM_2 eigenmodes with parallel and antiparallel phase and energy velocities [13]. We call the former a "forward (positive-index) mode" and the latter a "backward (negative-index) mode," and denote them as $|f\pm\rangle$ and $|b\pm\rangle$, respectively. Here the plus and minus signs indicate the direction of the energy flow relative to the z axis. The effective index of the eigenmodes is given as $n_{\text{eff}} = \beta/k_0$, where β is the propagation constant, and their energy velocity is defined as $v_E = \int S_z dx / \int u dx$, where u is the time-averaged energy density [19,20] and S_z is the time-averaged z component of the Poynting vector. Here the energy velocity is used to analyze the energy flow and energy density in dispersive and lossy media [20]. The energy velocity v_E coincides with the group velocity $v_g = d\omega/dk$ in lossless media, but this is not the case when loss is present and the wave vector is complex [19–21].

The effective index and energy velocity as a function of the waveguide core thickness are shown in Figs. 1(b) and 1(c), respectively. For the lossless case (blue curves), $|b\rangle$ modes carry zero energy if the core thickness lies outside the range $[\alpha_d, \alpha_c]$, where they become evanescent, while $|f\rangle$ modes propagate without loss if $\alpha > \alpha_d$. Furthermore, the forward and backward modes coalesce at the degeneracy point, leading to the mutual cancellation of energy flows, and hence zero group velocity [5]. Besides, the degeneracy point provides a perfect coupling between $|f\rangle$ and $|b\rangle$ modes as their wave vectors coincide. In the lossy case (red curves; $\gamma = 0.01$), forward and backward modes do not coalesce at the degeneracy point, so the energy velocity never goes to zero. However, the general behavior

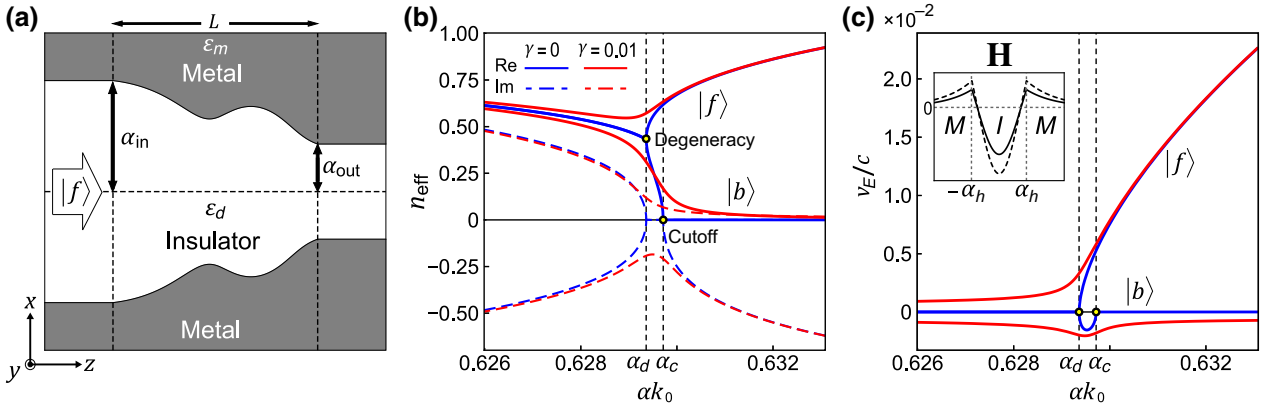

FIG. 1. (a) A free-form *M-I-M* light-trapping waveguide; the curvature is exaggerated. (b) Dispersion of the fundamental plasmonic modes supported by the *M-I-M* waveguide as a function of the half of the normalized core thickness αk_0: the real (solid lines) and imaginary (dashed lines) parts of the effective mode index for lossless (blue lines) and lossy (red lines) cases; metal loss $\gamma = 0.01$. (c) Corresponding energy velocity of the modes shown in (b); the inset shows the magnetic field profile inside the waveguide plotted for the forward-propagating (solid lines) and backward-propagating (dashed lines) TM_2 modes for core thickness $\alpha_h k_0 = (\alpha_d k_0 + \alpha_c k_0)/2$. Vertical dashed lines in (b),(c) indicate the core thickness when the degeneracy (α_d) and mode cutoff (α_c) conditions are satisfied.

of the group velocity and the effective index remains the same as in the lossless case: v_E reduces, and n_{eff} values of $|f\rangle$ and $|b\rangle$ modes get close to each other near the degeneracy point. Therefore, one can expect the degeneracy and cutoff behavior of modes to be preserved unless a fairly high loss is introduced.

B. Definition of the light-trapping quality factor

The quality factor Q for the light-trapping structure can be evaluated as the ratio between the total time-averaged energy U stored in the waveguide and the dissipated power P, all at the steady state: $Q=\omega U/P$. Q is directly proportional to the light-trapping time $\tau=Q/\omega$ [13], and can be understood as a measure of the temporal trapping performance. In the steady state, the dissipated power (due to absorption, reflection, and transmission) and incident power are equal, so P is equivalent to the incident power. We assume the input wave to be the $|f+\rangle$ mode, excited at the input port of the waveguide segment considered [Fig. 1(a)]. Then the total stored energy U can be obtained from the distribution of electromagnetic fields in the waveguide, obtained with the transfer-matrix method, taking into account the eigenmodes' propagation and coupling (for details on the transfer-matrix formalism, see Sec. S1 of Supplemental Material [18]). For the dispersive and dissipative medium (the metal claddings), according to the Loudon approach [19,20], the energy density is defined as $u(\omega)=\mu_0(|\mathbf{H}|^2/4)+\varepsilon_0(\text{Re}\,[\varepsilon_m]+2\text{Im}\,[\varepsilon_m]\omega/\,\Gamma)(|\mathbf{E}|^2/4)$. Assuming the Drude model for metal permittivity, $\varepsilon_m(\omega)=1-\omega_p^2/(\omega^2+i\Gamma\omega)$, where ω_p is the plasma frequency and Γ is the damping constant. Then the energy density in metal claddings is given by $u(\omega)=\mu_0(|\mathbf{H}|^2/4)+\varepsilon_0\{2-\text{Re}[\varepsilon_m(\omega)]\}|\mathbf{E}|^2/4$.

C. Numerical optimization for maximizing the quality factor

1. Demonstration for the trivial case and necessity for numerical optimization

One might expect that the reasonable approach to maximize the quality factor would be to design a light-trapping waveguide with constant core thickness, satisfying (or close to) the degeneracy condition when the group velocity of all modes is minimal. To check the validity of this argument, we start by simulating several waveguides of relatively long length $Lk_0=8$, $\gamma=0.004$, and different section of the waveguide having the degeneracy core thickness while keeping the same thickness of the input and output ports. The waveguide's core profile $\alpha(z)$ is designed to be monotonically decreasing while having its tangent line parallel to the z axis at the point where $\alpha(z=L_d)=\alpha_d$, which is fixed to that in the waveguide of linear profile at $L_dk_0=4.75$, as shown in Fig. 2(a). Then we use the following nth-order equation to describe the core profile $\alpha(z)\propto z^n$:

$$\alpha(z)=\frac{(-1)^n(\alpha_{\text{in}}-\alpha_d)}{L_d^n}(z-L_d)^n+\alpha_d,\quad z<L_d,$$

$$\alpha(z)=\frac{(\alpha_{\text{out}}-\alpha_d)}{(L-L_d)^n}(z-L_d)^n+\alpha_d,\quad z\geq L_d.$$

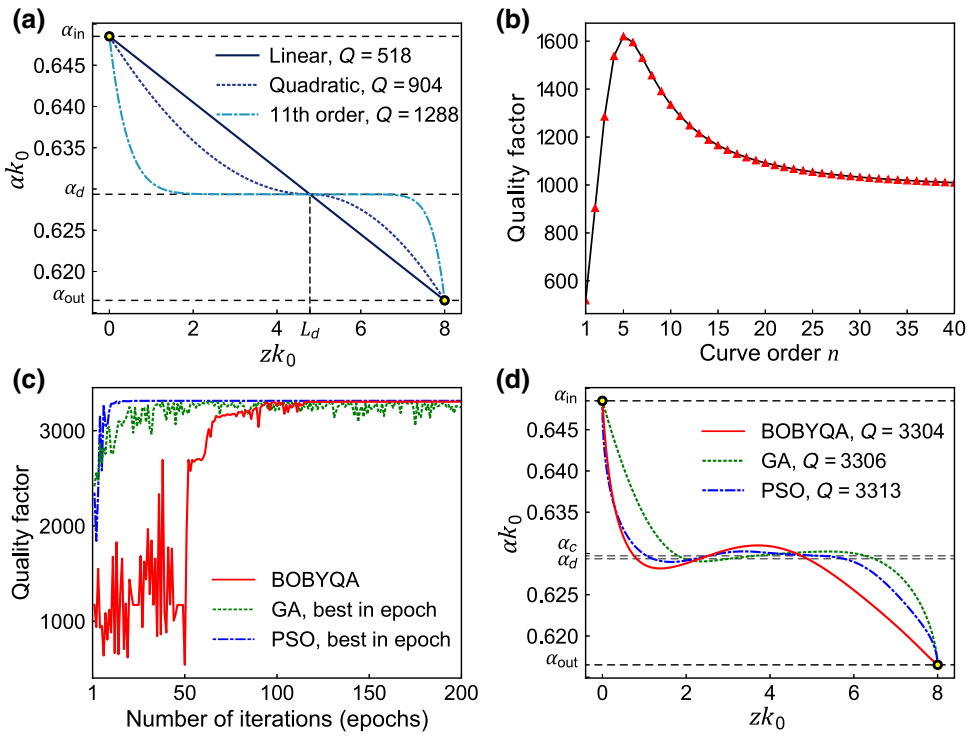

FIG. 2. (a) Profiles of the waveguide cladding for curve order $n=1$ (dark-blue solid line), $n=2$ (purple dotted lines), and $n=11$ (light blue dash-dotted line). (b) Quality factor as a function of n, calculated with the transfer-matrix method. (c) Optimization progress and (d) optimized waveguide profiles for BOBYQA (solid red line), GA (dotted green line), and PSO (dash-dotted blue line) algorithms. In (c), the best quality factor in each epoch is plotted for GA and PSO since they are pool-based algorithms.

We obtain the quality factor of the waveguides having a different curve order n, as demonstrated in Fig. 2(a). If Q increases with the section of the waveguide having the degeneracy thickness, then it should increase with the curvature order. However, as shown in Fig. 2(b), increasing the length of the segment having the degeneracy thickness does not significantly increase the quality factor compared with the simple linear taper ($Q = 518$). In fact, we observe a single peak value of $Q \approx 1600$ for the profile of fifth order, while Q reduces for the profiles of higher orders. This clearly demonstrates that merely increasing the length of the waveguide segment satisfying the degeneracy condition has limitations for increasing the quality factor. Because of the difficulty of designing the waveguide with high Q relying on intuition, and the absence of an analytical method to do so, we use an approach based on a waveguide of arbitrary shape that is numerically optimized to maximize Q.

2. Optimization methods and results

We perform the optimization using three different numerical algorithms to increase the probability of discovering the best-possible result: genetic algorithm (GA), particle-swarm optimization (PSO), and bound optimization by quadratic approximation (BOBYQA). A GA mimics the natural evolution process in order to find the global optimum by using selection, crossover, and mutation operations [22]. PSO uses the swarm of "particles" as initial optimization points to find the global optimum, while sharing the best "coordinates" between the members of the entire swarm [23]. BOBYQA searches for the local optimum on the basis of the trust-region method [24]. To parametrize an arbitrary waveguide profile, we use a Bezier curve with several control points. The optimization process is based on maximizing Q of the waveguide by changing the coordinates of the control points and thus varying the Bezier profile of the waveguide. The only restriction imposed on the points' coordinates is the core thickness limited by the size of the input (α_{in}) and output (α_{out}) ports. Use of as few as three control points (i.e., six parameters: three pairs of coordinates x and y) is enough to achieve the maximum values of Q. Details on the implementation of each numerical optimization method are given in Secs. S2–S4 of Supplemental Material [18].

Figure 2(c) shows the optimization progress for each method used, all demonstrating convergence to the same value of $Q \approx 3310$ (with less than 0.3% discrepancy), which is more than 6.4 times greater than that of the linearly tapered waveguide (of the same length and port sizes). The waveguide profiles obtained with the three different optimization methods are displayed in Fig. 2(d). Even though we do not impose any specific conditions on the cladding curvature, all three optimization methods arrive at similar shapes, all having an up-and-down wavelike feature around the points of degeneracy and cutoff.

The light-trapping performance of the optimized structure nearly reaches the theoretical limit, which validates the optimization results. We theoretically estimate this upper bound Q_{UB} as the maximum ratio between the electromagnetic energy of guided modes and the dissipated energy per optical cycle in an infinitely long parallel M-I-M waveguide with core thickness α among all possible combinations of $\alpha \in [\alpha_{\text{in}}, \alpha_{\text{out}}]$ and input modes ($|f\rangle$ and $|b\rangle$). Since an infinitely long parallel waveguide does not have energy loss by reflection or transmission, Q_{UB} can be interpreted as the inverse of the absorptive decay rate in the system. For the value of metal loss considered, $Q_{\text{UB}} = 3358$, which means that the solutions obtained (waveguide shapes) provide Q values as close to the theoretical limit as 99%.

D. Mechanism of optimized light trapping

To gain insight into the physics of the light trapping in the optimized M-I-M waveguide, we conduct full-wave FEM numerical simulations. We compare two cases: a linear waveguide and an optimized free-form waveguide obtained by the PSO algorithm (which provides the highest quality factor). First we confirm the convergence of Q calculated with the transfer-matrix method and FEM simulations, having less than 1% discrepancy. Then we obtain the distribution of the energy density u inside the waveguide for these two cases, as shown in Figs. 3(a) and 3(b), demonstrating much stronger field confinement in the optimized free-form waveguide. The energy density is maximal in the waveguide segment between the "inverse" [α_c, α_d] and "regular" [α_d, α_c] pairs of degeneracy and cutoff points (critical points) of the profile. The optimized waveguide geometry is practically indistinguishable from the linear case when plotted with comparable axis scales. This highlights that a tiny change in geometry results in a significant increase in the quality factor.

We analyze the behavior of each mode by calculating its mode amplitude. The mode amplitude $|a|$ is given as $|a|^2 = \left|\int dx(\boldsymbol{E} \times \boldsymbol{H})_z/2\right|$, where $\mathbf{E}$ and $\mathbf{H}$ are the electric and magnetic fields of the mode. If the mode is propagating without loss (having a real wave vector), then $|a|^2$ is the magnitude of the time-averaged Poynting vector (see Sec. S1 of Supplemental Material [18]). The spatial distribution of the mode amplitudes in the linear and optimized geometries is plotted in Figs. 3(c) and 3(d). In the linearly tapered waveguide, all four eigenmodes are excited in the narrow region within [α_d, α_c], and thus the major portion of the trapped energy resides near this area [13]. However, the mode amplitudes in the optimized waveguide exhibit an exotic behavior, associated with the presence of several critical points. As can be seen in Figs. 3(b) and 3(d), the existence of several critical points in the waveguide allows

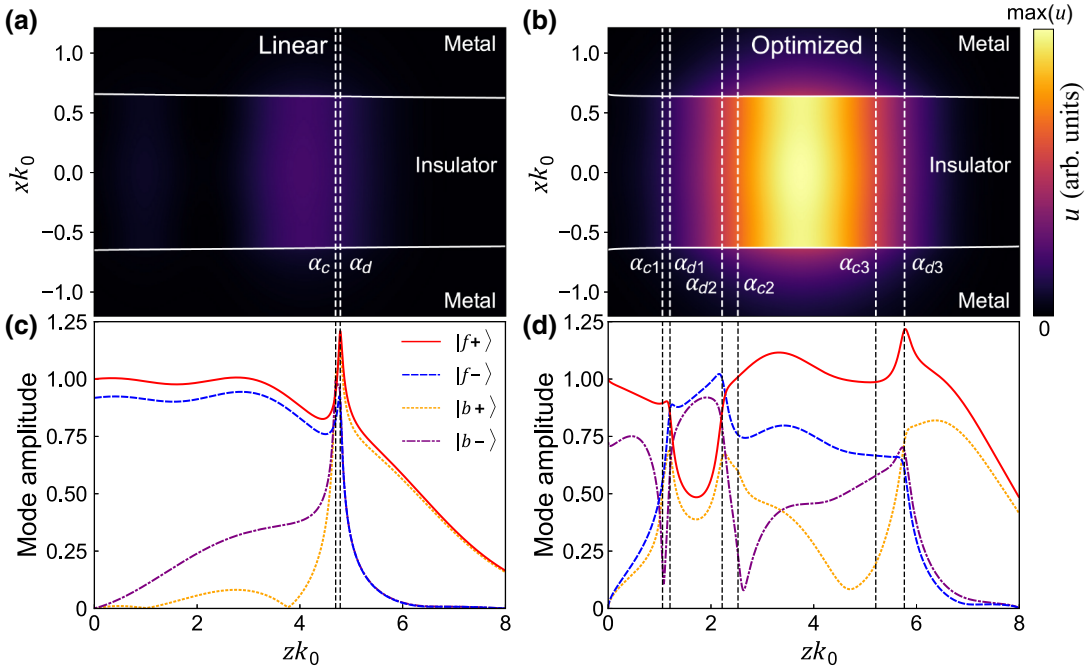

FIG. 3. Energy density $u(x,z)$ inside (a) the linear waveguide and (b) the optimized waveguide. Vertical dotted lines indicate the lateral positions where the core thickness corresponds to the degeneracy α_d and mode cutoff α_c. (c) Spatial distribution of the mode amplitudes $|a|$ for $|f+\rangle$ (solid red line), $|f-\rangle$ (dashed blue line), $|b+\rangle$ (dotted orange line), and $|b-\rangle$ (dash-dotted purple line) eigenmodes along the linear waveguide. (d) Same as in (c) for the optimized waveguide.

the formation of a multiple-boundary plasmonic "cavity" formed by three pairs of neighboring critical points [α_{c1}, α_{d1}], [α_{d2}, α_{c2}], and [α_{c3}, α_{d3}]. Here each pair of critical points [α_{ci}, α_{di}] ($i=1, 2, 3$) effectively acts as a mode-converting partial reflector, as $|f\rangle$ and $|b\rangle$ modes coincide at the degeneracy point α_d, and the mode cutoff α_c selectively reflects $|b\rangle$ modes. As a result, all $|f\rangle$ and $|b\rangle$ modes are simultaneously excited throughout the cavity, leading to significantly enhanced light-trapping performance.

Another important way to compare the two waveguides is to analyze mechanisms of power flow and energy loss. Because the coupling to the higher-order modes is negligible in an adiabatically varying waveguide, there are three loss channels in the light-trapping geometry: absorption, reflection, and transmission loss. Absorption (Ohmic) loss P_{abs} in a metal can be evaluated by integrating the density of dissipated power $\varepsilon_0\gamma|\mathbf{E}|^2/2$ over the waveguide structure [19]. Reflection loss is the power leaving the waveguide through the input port via the reflected modes and can be calculated as $P_r = P - \int S_z(x,0)dx$, where $S_z(x,0)$ is the z component of the Poynting vector evaluated at the input port ($z=0$) at steady state. Transmission loss $P_t = \int S_z(x,L)dx$ is the net power flow of the waveguide's output port and is nearly zero, because the narrow waveguide ($\alpha < \alpha_d$) does not support propagating modes [Fig. 1(b); note that $P_t = 0$ in the lossless case]. Combining the reflection and transmission losses, we define the energy loss through the guided waves as $P_g = P_r + P_t$. As shown in Fig. 3(d), the optimized waveguide is critically coupled to the incident wave and has zero mode amplitude for $|f-\rangle$ at the entrance, leading to zero guided-wave loss. In this case, all incident power is dissipated solely via the Ohmic loss in the metal claddings. In contrast, for the linearly tapered waveguide, nearly 84% of the incident energy is reflected and only 16% is absorbed. Because the absorptive decay rate for both structures is similar, this can be translated into a 6.3 times faster total decay rate, which is consistent with the ratio between the quality factors of the linear and optimized waveguides.

E. Dependence of the quality factor on metal loss and waveguide length

The maximum achievable quality factor $Q(\gamma,L)$ monotonically increases with decreasing γ and increasing L of the waveguide as shown in Fig. 4(a). Here $Q(\gamma,L)$ is obtained by our individually conducting numerical optimization for each pair of γ and L. When the waveguide is sufficiently long, the optimal structure has negligible guided-wave loss $P_g \approx 0$, and the absorption loss dominates the system. Consequently, the optimized quality factor $Q(\gamma)$ is inversely proportional to γ and tends to diverge in the limiting case of the lossless system ($\gamma \to 0$) as shown by the solid black line in Fig. 4(b) for $Lk_0 = 8.0$. On the other hand, when the waveguide is too short to achieve the critical coupling to the incident light, the guided-wave

loss P_g is no longer negligible and competes with the absorptive decay channel P_{abs}. As L decreases, absorption becomes negligible compared with the guided-wave loss ($P_{abs} \ll P_g$), and $Q(\gamma)$ quickly saturates; the solid red curve in Fig. 4(b) demonstrates this for $Lk_0 = 2$.

To systematically unravel the contribution of each loss channel, we decompose the total normalized decay rate $\Gamma_{tot} \equiv 1/Q = P_{tot}/\omega U$ of the optimized waveguides into the absorptive decay rate ($\Gamma_{abs} \equiv P_{abs}/\omega U = 1/Q_{abs}$) and the guided-wave decay rate ($\Gamma_g \equiv P_g/\omega U = 1/Q_g$), as shown in Figs. 4(c) and 4(d), respectively. The quality factor of the system is then given by $Q = 1/(\Gamma_{abs} + \Gamma_g)$. We find Γ_{abs} to be nearly independent of L and directly proportional to the material loss, $\Gamma_{abs} \propto \gamma$, as can be seen in Fig. 4(d). On the other hand, Γ_g is almost independent of γ, and rapidly decreases with increasing L, as plotted in Fig. 4(c). In sharp contrast to the linearly tapered waveguide, where Γ_g is simply proportional to $1/L$ [13], the optimized light-trapping structure exhibits a fundamentally different behavior as its guided-wave decay rate is exponentially dependent on L.

The nontrivial dependence on Γ_g on L allows the quality factor of the optimized structure to saturate at a surprisingly short device length. To demonstrate this, we characterize the saturation behavior by plotting $Q(\gamma,L)$ normalized by the long-cavity limit $Q_\infty(\gamma) \equiv Q(\gamma, Lk_0 = 8)$, as shown in Fig. 5(a). This saturation behavior can be understood as competition between $\Gamma_g(L)$ and $\Gamma_{abs}(\gamma)$. As L increases, Γ_g drops and the system eventually becomes dominated by the absorption loss, while the quality factor saturates at $Q \approx 1/\Gamma_{abs}(\gamma)$. To numerically evaluate the saturation of Q, we introduce the characteristic waveguide length $L_c(\gamma)$ necessary for the optimization convergence to $Q = Q_\infty(\gamma)/2$, corresponding to $\Gamma_g(L_c) \approx \Gamma_{abs}(\gamma)$. For $\gamma = 0.003$, the characteristic length $L_c k_0 = 2.5$, which is only 4.0 times the wavelength in the dielectric medium, and is 5.6 times shorter than the propagation length of the $|f+\rangle$ mode at the degeneracy point. $L_c(\gamma)$ increases as the metal becomes less lossy, but the dependence is not strong as in the case of linear tapers. For example, the characteristic length for $\gamma = 0.3$ and 0.001 is $L_c k_0 = 0.75$ and 2.85, respectively; $L_c(\gamma)$ increases by only 3.8 times, while γ decreases by 300 times. As demonstrated in Fig. 5(b), we find that $L_c(\gamma)$ logarithmically scales with γ^{-1}. Because the characteristic length L_c of a linearly tapered waveguide linearly scales with γ^{-1}, the logarithmic scaling law is an extraordinary property of the optimized waveguide that would significantly reduce the device footprint necessary for light trapping. The same behavior is also observed in the *I-M-I* light-trapping geometry (see Sec. S5 of Supplemental Material [18]); therefore, we speculate that the logarithmic scaling law of the characteristic length with the metal loss is a general property of optimized free-form waveguides, stemming from the exponential suppression of guided-wave loss due to the formation of a cavity with efficient mode conversion. Because of the small device

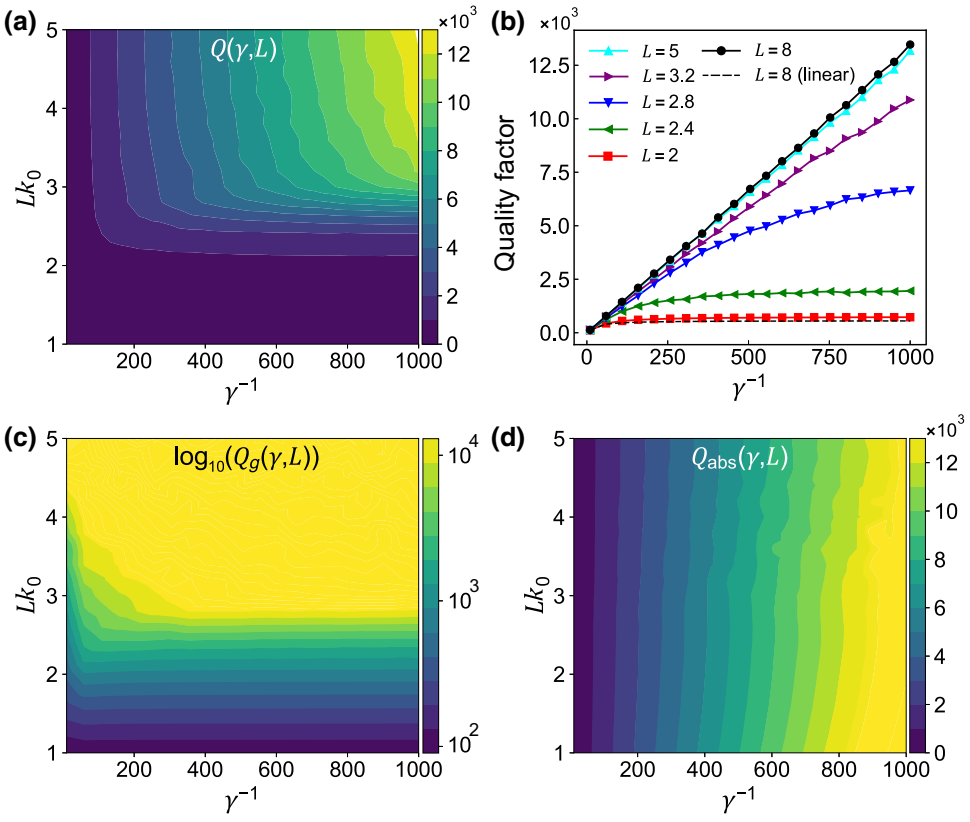

FIG. 4. (a) Optimized quality factor as a function of waveguide length L and Ohmic loss γ. (b) Optimized quality factor as a function of γ for different values of Lk_0. (c) Logarithm of the inverse guided-wave decay rate $Q_g = 1/\Gamma_g$ as a function of L and γ. (d) Same as in (c) for the inverse absorptive decay rate $Q_{abs} = 1/\Gamma_{abs}$. All data are obtained with the transfer-matrix method.

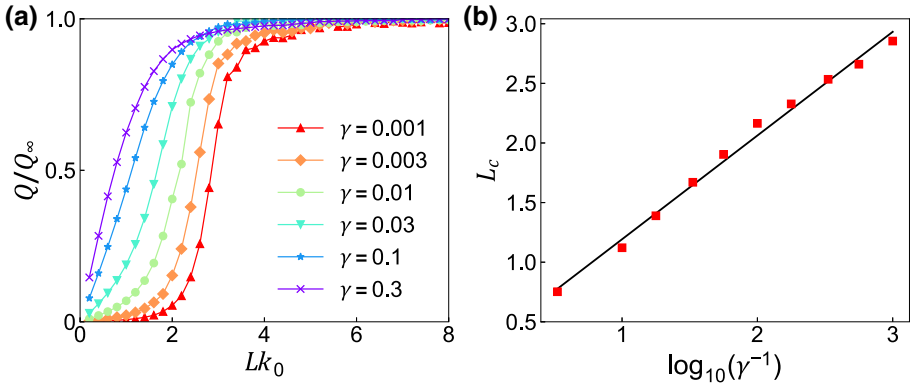

FIG. 5. (a) Normalized quality factor as a function of the waveguide length L and the Ohmic loss γ. (b) Characteristic waveguide length L_c versus inverse logarithm of γ.

footprint $A \leq 0.2\lambda_0^2$, the optimized M-I-M waveguides exhibit $Q/A \sim (10^3$–$10^5)\lambda_0{}^{-2}$ depending on the metal loss, which is comparable to state-of-the-art photonic cavities such as ultrahigh-Q microring resonators [25,26] (for details of the mode volume calculation, see Sec. S6 of Supplemental Material [18]).

F. Optimized waveguide with realistic materials

As demonstrated above, the Ohmic loss in metal claddings plays a key role in limiting the light-trapping quality factor. Therefore, proper selection of materials is crucial to achieve high Q in real devices. In this section, we briefly discuss the optimization results obtained with realistic materials at visible and mid-IR frequencies, and provide a perspective on the possible device configuration for the terahertz regime.

For the frequency of the visible free-space wavelength of 400 nm, we design the M-I-M waveguide using titanium dioxide [27] ($\epsilon \approx 7.09 + 0.002i$) and low-loss single-crystal silver [28] ($\epsilon \approx -1.7 + 0.15i$). Such a M-I-M waveguide supports both negative-index and positive-index modes at a given frequency, and therefore can be used for light trapping (see Sec. 2.1 for details). The optimized $Ag/TiO_2/Ag$ waveguide exhibits $Q = 82.3$, which is 2.2 times larger than in the linearly tapered case, $Q = 37.1$. For the mid-IR frequency corresponding to the free-space wavelength of 11 μm, many dielectric materials with negligible loss are available, but we use undoped germanium [29] for its large permittivity ($\epsilon \approx 16.01$). As a material with small negative permittivity, we select polar dielectric silicon carbide [30,31] ($\epsilon \approx -3.8 + 0.125i$). The optimized SiC/Ge/SiC waveguide demonstrates $Q = 198.7$, which is 5.2 times greater than in the linearly tapered case, $Q = 38.2$. However, as we demonstrate in Sec. S7 of Supplemental Material [18], only the waveguide designed for the mid-IR frequencies has feasible micrometer-scale dimensions, while the device designed for visible frequencies would require subnanometer variation of the core profile.

For the terahertz regime, we speculate that low-loss "spoof plasmons" at patterned metal interfaces [32] can be potentially used for light trapping in patterned M-I-M waveguides [33,34]. In this frequency range, the large plasmon wavelength can be beneficial for fabrication of large-scale devices. Fabrication of patterned metallic surfaces as well as free-form waveguides with very high precision and very low scattering might be possible with, for example, a modified version of the ultraprecise laser-based "SNAP" technique [35,36].

III. CONCLUSION

In summary, we demonstrate that the light-trapping performance of plasmonic nanostructures can be significantly improved and reach the theoretical limit by optimizing the waveguide geometry. Through the systematic analyses of the loss channels, we explain the peculiar dependence of the trapping quality factor on the structural and material parameters in terms of the two competing though practically independent energy-dissipation mechanisms: the absorptive (Ohmic) decay and the guided-wave decay. For the optimized structures, we observe the guided-wave decay rate to be logarithmically dependent on the length of the structure, which is fundamentally different from the case of conventional linearly tapered waveguides. As a result, the quality factor of the free-form optimized structure reaches the material-loss-limited Q at a surprisingly short device length, several times shorter than the propagation length of the guided modes. The high quality factor and extremely small device footprint of the optimized light-trapping structure make it an ideal platform for waveguide-compatible strong light-matter interaction. Finally, we discuss the performance of waveguide designs with realistic materials at visible and mid-IR frequencies. We expect further study will lead to the realization of compact elements for integrated photonic circuits.

ACKNOWLEDGMENTS

This research was supported by the National Research Foundation of Korea (NRF) funded by Ministry of Science and ICT (Grants No. 2017R1E1A1A01074323 and

No. 2016M3D1A1900038). S.G.M. acknowledges support from the NRF Young Researchers program (Grant No. 2019R1C1C1011131) funded by the Ministry of Science and ICT.

[1] T. Baba, Slow light in photonic crystals, Nat. Photonics **2**, 465 (2008).
[2] T. F. Krauss, Slow light in photonic crystal waveguides, J. Phys. D. Appl. Phys. **40**, 2666 (2007).
[3] K. L. Tsakmakidis, O. Hess, R. W. Boyd, and X. Zhang, Ultraslow waves on the nanoscale, Science **358**, eaan5196 (2017).
[4] J. T. Mok and B. J. Eggleton, Expect more delays, Nature **433**, 811 (2005).
[5] K. L. Tsakmakidis, A. D. Boardman, and O. Hess, "Trapped rainbow" storage of light in metamaterials, Nature **450**, 397 (2007).
[6] T. Jiang, J. Zhao, and Y. Feng, Stopping light by an air waveguide with anisotropic metamaterial cladding, Opt. Express **17**, 170 (2009).
[7] M. I. Stockman, Nanofocusing of Optical Energy in Tapered Plasmonic Waveguides, Phys. Rev. Lett. **93**, 137404 (2004).
[8] J. He, Y. Jin, Z. Hong, and S. He, Slow light in a dielectric waveguide with negative-refractive-index photonic crystal cladding, Opt. Express **16**, 11077 (2008).
[9] Y. Shen, J. Fu, and G. Yu, Rainbow trapping in one-dimensional chirped photonic crystals composed of alternating dielectric slabs, Phys. Lett. A **375**, 3801 (2011).
[10] Q. Gan, Y. J. Ding, and F. J. Bartoli, "Rainbow" Trapping and Releasing at Telecommunication Wavelengths, Phys. Rev. Lett. **102**, 056801 (2009).
[11] Q. Gan, Y. Gao, K. Wagner, D. Vezenov, Y. J. Ding, and F. J. Bartoli, Experimental verification of the rainbow trapping effect in adiabatic plasmonic gratings, Proc. Natl Acad. Sci. **108**, 5169 (2011).
[12] Q. Gan, Z. Fu, Y. J. Ding, and F. J. Bartoli, Ultrawide-Bandwidth Slow-Light System Based on THz Plasmonic Graded Metallic Grating Structures, Phys. Rev. Lett. **100**, 256803 (2008).
[13] M. S. Jang and H. Atwater, Plasmonic Rainbow Trapping Structures for Light Localization and Spectrum Splitting, Phys. Rev. Lett. **107**, 207401 (2011).
[14] J. Zhu, Y. Chen, X. Zhu, F. J. Garcia-Vidal, X. Yin, W. Zhang, and X. Zhang, Acoustic rainbow trapping, Sci. Rep. **3**, 1728 (2013).
[15] X. P. Zhao, W. Luo, J. X. Huang, Q. H. Fu, K. Song, X. C. Cheng, and C. R. Luo, Trapped rainbow effect in visible light left-handed heterostructures, Appl. Phys. Lett. **95**, 071111 (2009).
[16] W. T. Lu, Y. J. Huang, B. D. F. Casse, R. K. Banyal, and S. Sridhar, Storing light in active optical waveguides with single-negative materials, Appl. Phys. Lett. **96**, 211112 (2010).
[17] G. Wang, H. Lu, and X. Liu, Gain-assisted trapping of light in tapered plasmonic waveguide, Opt. Lett. **38**, 558 (2013).
[18] See Supplemental Material at http://link.aps.org/supplemental/10.1103/PhysRevApplied.12.024030 for details on the transfer-matrix formalism (Sec. S1), optimization procedure (Secs. S2-S4), analysis of the optimized *I*-*M*-*I* waveguide (Sec. S5), quality-factor-to-mode-volume ratio (Sec. S6), and optimization results with realistic materials (Sec. S7).
[19] F. D. Nunes, T. C. Vasconcelos, M. Bezerra, and J. Weiner, Electromagnetic energy density in dispersive and dissipative media, J. Opt. Soc. Am. B **28**, 1544 (2011).
[20] R. Loudon, Propagation of electromagnetic energy through an absorbing dielectric, J. Phys. A: Gen. Phys. **3**, 233 (1970).
[21] R. Ruppin, Electromagnetic energy density in a dispersive and absorptive material, Phys. Lett. A **299**, 309 (2002).
[22] K. Deb, *Multi-Objective Optimization Using Evolutionary Algorithms* (John Wiley & Sons Inc., New York, NY, USA, 2001).
[23] R. C. Eberhart and Y. Shi, Particle swarm optimization: developments, applications and resources, in Proc. 2001 Congr. Evol. Comput. (IEEE Cat. No.01TH8546) (IEEE, 2001), pp. 81–86.
[24] M. J. D. Powell, The BOBYQA algorithm for bound constrained optimization without derivatives, Cambridge NA Rep. NA2009/06, Univ. Cambridge, Cambridge 26 (2009).
[25] H. Lee, T. Chen, J. Li, K. Y. Yang, S. Jeon, O. Painter, and K. J. Vahala, Chemically etched ultrahigh-Q wedge-resonator on a silicon chip, Nat. Photonics **6**, 369 (2012).
[26] M. Zhang, C. Wang, R. Cheng, A. Shams-Ansari, and M. Loncar, Monolithic ultrahigh-Q lithium niobate microring resonator, Optica **4**, 1536 (2017).
[27] T. Siefke, S. Kroker, K. Pfeiffer, O. Puffky, K. Dietrich, D. Franta, I. Ohlidal, A. Szeghalmi, E.-B. Kley, and A. Tunnermann, Materials pushing the application limits of wire grid polarizers further into the deep ultraviolet spectral range, Adv. Opt. Mater. **4**, 1780 (2016).
[28] T. Mori, T. Mori, M. Fujii, Y. Tominari, A. Otomo, and K. Yamaguchi, Optical properties of low-loss Ag films and nanostructures on transparent substrates, ACS Appl. Mater. Interfaces **10**, 8333 (2018).
[29] H. H. Li, Refractive index of silicon and germanium and its wavelength and temperature derivates, J. Phys. Chem. Ref. Data **9**, 561 (1980).
[30] J. D. Caldwell, L. Lindsay, V. Giannini, I. Vurgaftman, T. L. Reinecke, S. A. Maier, and O. J. Glembocki, Low-loss, infrared and terahertz nanophotonics using surface phonon polaritons, Nanophotonics **4**, 44 (2015).
[31] J. D. Caldwell, G. J. Orest, Y. Francescato, N. Sharac, V. Giannini, F. J. Bezares, J. P. Long, J. C. Owrutsky, I. Vurgaftman, J. G. Tischler, V. D. Wheeler, N. D. Bassim, L. M. Shirey, R. Kasica, and S. A. Maier, Low-loss, extreme sub-diffraction photon confinement via silicon carbide localized surface phonon polariton resonators, Nano Lett. **13**, 3690 (2013).
[32] J. B. Pendry, L. Martin-Moreno, and F. J. Garcia-Vidal, Mimicking surface plasmons with structured surfaces, Science **305**, 847 (2004).

[33] M. A. Kats, D. Woolf, R. Blanchard, N. Yu, and F. Capasso, Spoof plasmon analogue of metal-insulator-metal waveguides, Opt. Exp. **19**, 14860 (2011).

[34] Y. Yang, X. Shen, P. Zhao, H. C. Zhang, and T. J. Cui, Trapping surface plasmon polaritons on ultrathin corrugated metallic strips in microwave frequencies, Opt. Exp. **23**, 7031 (2015).

[35] M. Sumetsky and Y. Dulashko, SNAP: Fabrication of long coupled microresonator chains with sub-angstrom precision, Opt. Exp. **20**, 27896 (2012).

[36] M. Sumetsky, K. Abedin, D. J. DiGiovanni, Y. Dulashko, J. M. Fini, and E. Monberg, Coupled high Q-factor surface nanoscale axial photonics (SNAP) microresonators, Opt. Lett. **37**, 990 (2012).